RSC Advances

This is an *Accepted Manuscript*, which has been through the Royal Society of Chemistry peer review process and has been accepted for publication.

Accepted Manuscripts are published online shortly after acceptance, before technical editing, formatting and proof reading. Using this free service, authors can make their results available to the community, in citable form, before we publish the edited article. This *Accepted Manuscript* will be replaced by the edited, formatted and paginated article as soon as this is available.

You can find more information about *Accepted Manuscripts* in the Information for Authors.

Please note that technical editing may introduce minor changes to the text and/or graphics, which may alter content. The journal's standard Terms & Conditions and the Ethical guidelines still apply. In no event shall the Royal Society of Chemistry be held responsible for any errors or omissions in this *Accepted Manuscript* or any consequences arising from the use of any information it contains.

ROYAL SOCIETY OF CHEMISTRY

www.rsc.org/advances

Transition from Rings to Spots in a Precipitation Reaction-Diffusion System †

Malak Dayeh,[a] Manal Ammar,[a] and Mazen A–Ghoul*[a]

Received Xth XXXXXXXXXX 20XX, Accepted Xth XXXXXXXXX 20XX
First published on the web Xth XXXXXXXXXX 200X
DOI: 10.1039/b000000x

We report for the first time the transition from rings to spots with squared/hexagonal symmetry in a periodic precipitation system, which consists of sulfide/hydroxide ions diffusing into a gel matrix containing dissolved cadmium (II) ions. A phase diagram delineating the onset of the transition and the regions of various patterns is presented. The transition threshold, wavelength, and size of the resulting spots are shown to be controllable by adjusting the initial concentrations of the diffusing electrolytes. A scenario analogous to spinodal decomposition using the Cahn-Hilliard equation is shown to capture the experimental results.

Pattern formation and self-organizing phenomena have attracted a considerable scientific interest due to their widespread applications in biology [1–4], chemistry [5], physics [6], and materials science [7]. A particular example of such phenomena is the periodic precipitation pattern discovered by R. E. Liesegang in 1896 [8,9], which exhibits precipitation bands (1D) and rings (2D). Ever since, different structures have been experimentally obtained and reported; these include: the unusual bands with revert spacing [10], bands with secondary structures [11], fractals [12], spirals [13], and 3D helices [14]. Recently, they have been applied in modern micro- and nanotechnology [15,16], and the control and engineering of these patterns represent a crucial task [17]. Noticeably, all of these patterns are based on the topologies of bands or rings and their modulations, and no other topologies have ever been observed despite that multi-lattice patterns, dislocations and broken filaments have been obtained in polycentric systems [18,19]. In this paper, we report for the first time the formation of a new precipitation pattern observed in the cadmium sulfide/hydroxide precipitation system, which displays a transition from parallel rings to spots with squared and hexagonal symmetry. The transition threshold, the prevalence of spots versus rings, the wavelength of the selected pattern, and the size of the spots can be controlled by the initial concentrations of the inner and outer electrolytes.

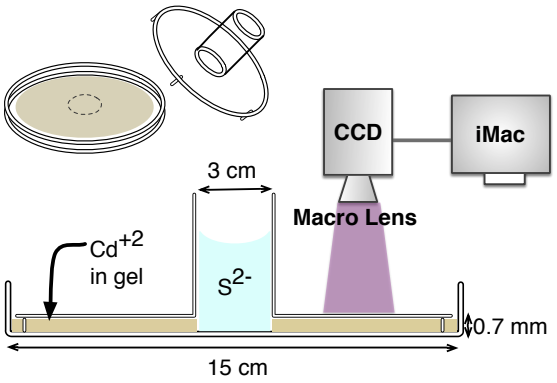

Fig. 1 A sketch of the experimental setup. It consists of a circular Plexiglass reactor (diameter= 15 cm) and a transparent Plexiglass cover (diameter= 12 cm) equipped with spacers in order to achieve a homogeneous gel matrix (5% gelatin containing the cadmium ions) of thickness 0.7 mm. The sulfide ions are then added to the central reservoir (diameter= 3 cm) mounted in the middle of the reactor. The patterns and their evolution are captured by a mounted CCD camera interfaced with a computer.†

Using the experimental setup and procedure described in Fig. 1, the spatio-temporal evolution of the system is initiated directly after the sulfide solution is diffused into the cadmium-doped gel. The dissolution process of sodium sulfide in water, described in (R_1), releases hydroxide ions (OH^-). In a high pH medium, the production of the sulfide ions also becomes appreciable as shown in (R_2). Since the diffusion coefficient of the hydroxide ions is about four times greater than that of the hydrogen sulfide (HS^-) and sulfide (S^{2-}) ions, a white precipitate is formed at the liquid-gel interface first, indicating a spontaneous reaction between the diffusing hydroxide ions and the cadmium ions (Cd^{2+}) existing in the pores of the gel (R_3). For a given set of initial inner and outer concentrations, the precipitation of $Cd(OH)_2$ exhibits concentric rings (Figs. 2A or 4A) at early times of evolution. As time progresses,

† Electronic Supplementary Information (ESI) available: Detailed experimental procedure and a movie exhibiting transition from rings to spots in addition to the ion-exchange yellow back-front. See DOI: 10.1039/b000000x/

[a] *Department of Chemistry, American University of Beirut, P.O.Box 11-0236, Riad El-Solh 1107 2020, Beirut, Lebanon. Fax: 961 1 365 217; Tel: 961 1 350 000; E-mail: mazen.ghoul@aub.edu.lb*

RSC Advances Accepted Manuscript

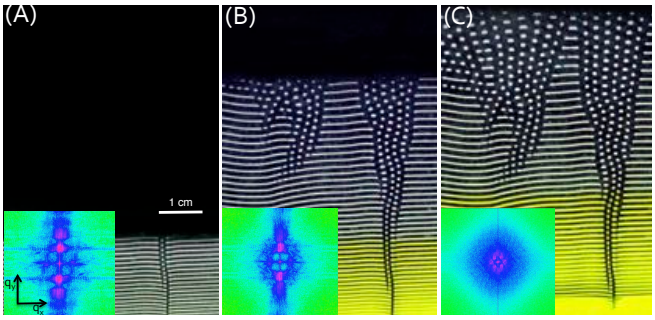

Fig. 2 Transition from Rings to Spots. (A) $t = 6\,hrs$; (B) $t = 18\,hrs$; (C) $t = 26\,hrs$. The inset figures are the 2D power spectra of the displayed patterns. The purple color indicates highest modes expressed in the pattern. Transition from stripes (A) to hexagonal pattern (C) is reflected in the power spectrum where the aligned wavenumbers along q_y in (A) are changed into 6 wavenumbers in (C) with a hexagonal symmetry.

white spots start appearing as defects among the rings in several locations as shown in Fig. 2A. They start multiplying and propagating in the direction of the diffusion front (Fig. 2B). Eventually, the whole domain of the reactor is invaded with such an unexpected pattern as shown in Fig. 2C†. The investigation of the time evolution of the power spectra of the patterns in Fig. 2 (insets) reveals the transition from bands to spots possessing a mixture of squared and hexagonal symmetry. It is noticeable that in the resulting pattern the distance between consecutive spots seems to increase as the distance from the center of the reactor increases towards its boundaries. Moreover, the spatial evolution of the white solid is followed by a yellow back-front resulting from the formation of yellow cadmium sulfide CdS due to the anionic exchange between OH^- and $S^{2-}(R_4)$, owing to the higher thermodynamic stability of the sulfide. This ion exchange is shown to be diffusion-limited. All underlying chemical reactions are summarized as follows:

$$Na_2S(s) \xrightarrow{H_2O} 2Na^+(aq) + HS^-(aq) + OH^-(aq) \qquad (R_1)$$

$$HS^-(aq) \xrightarrow{H_2O} S^{2-}(aq) + H_3O^+(aq) \qquad (R_2)$$

$$Cd^{2+}(gel) + 2OH^-(aq) \longrightarrow Cd(OH)_2(s) \qquad (R_3)$$

$$Cd(OH)_2(s) + S^{2-}(aq) \longrightarrow CdS(s) + 2OH^-(aq) \qquad (R_4)$$

Pattern control and selection is studied and a phase diagram is constructed. To detect the effect of the concentrations of the inner and outer electrolytes on the pattern morphology, five sets of different outer concentrations (varying between 200

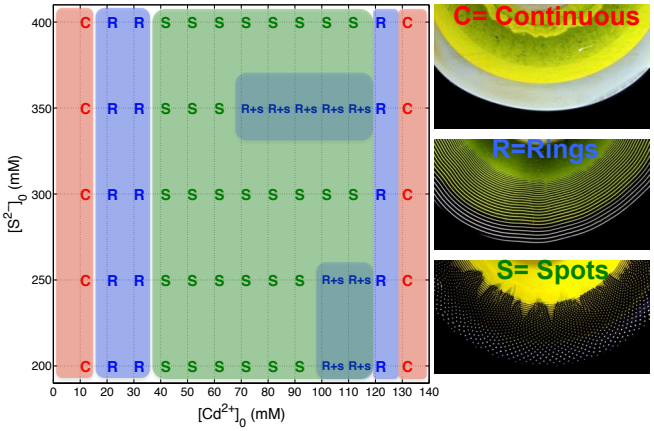

Fig. 3 Phase diagram representing the different morphologies obtained upon varying the inner and outer concentrations. **C**= continuous precipitation band; **R**= precipitation rings; **S**= spots. The **R+s** (lowercase **s**) on the phase diagram indicates occurrence of rings with some spots.

mM and 400 mM) are prepared, each containing 14 reactors at different inner concentrations (varying between 10 mM and 140 mM), using the same experimental procedure described in Fig. 1. The type of the emerging patterns are then grouped in the phase diagram shown in Fig. 3. At low cadmium concentration (less than 20 mM), only a continuous precipitating white front of $Cd(OH)_2$ is obtained without any rings or spots. A diffusing yellow back-front indicating the formation of CdS then follows. This regime is denoted by '**C**'. When the inner concentration is increased from 10 mM to 20 mM for all outer concentrations in the aforementioned range, clearly separated thin rings of a white/yellow precipitate are observed. This regime is denoted by '**R**'. Upon increasing the concentration of cadmium from 30 mM to 60 mM, numerous well-resolved spots with squared/hexagonal symmetry emerge just after the formation of a few rings. This region is labeled '**S**'. When the inner concentration increases beyond 60 mM, the structure of the phase diagram gets more complex, resulting in a mixture of predominating rings and some spots (denoted as '**R+s**') for outer concentrations ranging between 200 mM and 250 mM, and at around 350 mM. For inner concentration between 120 mM and 130 mM, we get back to the '**R**' regime but with thicker and fewer rings than what is obtained on the left-hand side of the phase diagram. For concentrations higher than 130 mM, we go back to the continuous precipitation zone.

The effect of inner and outer concentrations is further investigated. If we move horizontally across the phase diagram at a fixed outer concentration $[S^{2-}]_0$ = 400 mM, as shown in Fig. 3, starting at an inner concentration $[Cd^{+2}]_0$ = 30 mM, well-resolved thin rings are obtained (Fig. 4A). By increasing the inner concentration from 30 mM to 60 mM, a transition

RSC Advances Accepted Manuscript

This journal is © The Royal Society of Chemistry [year]

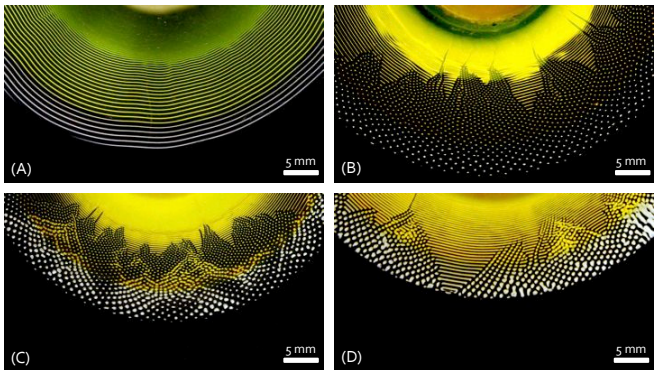

Fig. 4 The evolution of precipitation patterns within 48 hours at constant outer concentration $[S^{2-}]_0$ = 400 mM and various inner concentrations $[Cd^{2+}]_0$: (A)= 30 mM, (B)= 60 mM, (C)= 90 mM, (D)= 110 mM; Gelatin= 5%; Temp= 22 °C.

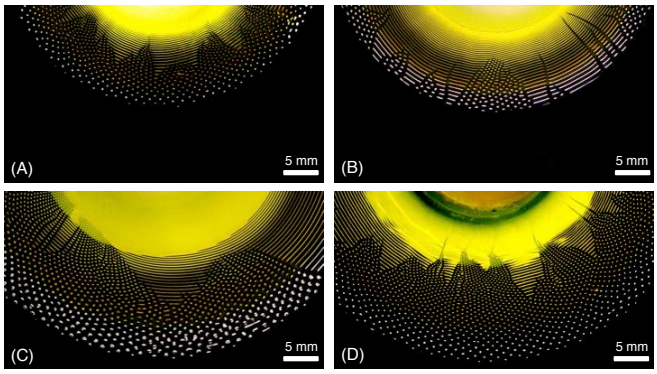

Fig. 5 The evolution of precipitation patterns within 48 hours at constant inner concentration $[Cd^{2+}]_0$ = 60 mM and various outer concentrations $[S^{2-}]_0$: (A)= 200 mM, (B)= 250 mM, (C)= 350 mM, (D)= 400 mM; Gelatin= 5%; Temp= 22 °C.

from thin rings to spots is clearly exhibited in Fig. 4B, and the resulting pattern after 48 hours is clearly dominated by spots with a squared/hexagonal symmetry. Further increase in the inner concentration to 90 mM (Fig. 4C) and to 110 mM (Fig. 4D) results in the formation of larger and closer spots until they all merge together at a concentration beyond 130 mM to form a continuous band as shown on the phase diagram. In analogy to Liesegang rings, the obtained spots are labeled by their number n along a special line of symmetry chosen to pass through them and starting at the first spot appearing in the system. To quantify, the size of a spot is given in terms of the measured area it occupies. In the case of Fig. 4B, the spot size changes almost linearly with n with values ranging from 0.1 mm^2 to 0.32 mm^2, whereas in the case of Fig. 4C, the spot size ranges from 0.45 mm^2 to 1.44 mm^2, and from 0.91 mm^2 to 2.6 mm^2 in the case of Fig. 4D. Therefore, the spots are shown to increase in size with the increase of the inner concentration. On the other hand, moving vertically in the phase diagram, the effect of varying the outer concentration does not noticeably affect the spot size, but it directly influences the spacing between spots and the distance they cover. Figure (5) shows that the increase in the outer concentration at a fixed inner concentration $[Cd^{2+}]_0$ =60 mM results in a faster reaction-diffusion process, thus allowing the precipitation and formation of closer spots that cover larger distances.

In order to shed more light on the control of the spots, the spacing between consecutive spots is measured for two sets of plates: *Set (I)* is prepared at constant outer concentration ($[S^{2-}]_0$ = 250 mM) with different inner concentrations $[Cd^{2+}]_0$ ranging between 40 mM and 80 mM, and *Set (II)* is prepared at constant inner concentration ($[Cd^{2+}]_0$ = 60 mM) with different outer concentrations $[S^{2-}]_0$ ranging between 200 mM and 350 mM. The spacing in a given pattern with spots is defined as $\lambda_n = x_{n+1} - x_n$ where x_n and x_{n+1} are the locations of spot n and the following one, $n+1$. Consequently, for *Set (I)*, the obtained five curves in Fig. 6A for λ_n versus n exhibit a linear relationship with a positive slope that increases with a decrease of the inner concentration. As for *Set (II)*, a linear direct spacing law is also obtained as shown in Fig. 6B, but with a positive slope increasing with a decrease in the outer concentration. Moreover, a spacing law for spots can be verified by computing the ratio $r = x_{n+1}/x_n$, which is written as $r = 1 + p$ with p ranging between 0.09 and 0.16 for *Set (I)* and between 0.13 and 0.08 for *Set (II)*. This observation is similar to the direct spacing law encountered in Liesegang banding systems[20,21], whereby the rate of diffusion increases with the increase of the outer electrolyte concentration[22], thus resulting in spots forming at closer distances than those with a lower outer concentration. On the other hand, the increase in the spot size with the increase in the inner concentration results in the formation of closer and bigger spots until they merge, which leads to smaller values of p. On that account, the initial concentrations of reactants provide suitable spatial control parameters for the spots. By the same token, a time law[23] is also observed whereby the ratio of x_n^2/t_n, where t_n is time elapsed until the formation on the nth band, is found to lead to a constant value at large n for all initial inner and outer concentrations.

The exact mechanism of Liesegang structure is still under investigation[24], and there has never been any unified model able to explain every experimental finding. However, researchers have agreed on two explanatory models: the pre-nucleation model based on the Ostwald supersaturation-nucleation-depletion cycle[25,26], and the post-nucleation model based on Ostwald ripening mechanism[27,28]and the Lifshitz-Slyozov instability[29]. Some researchers have also combined both models to describe some of the aforementioned precipitation patterns[30]. Another important mean-field theory that

RSC Advances Accepted Manuscript

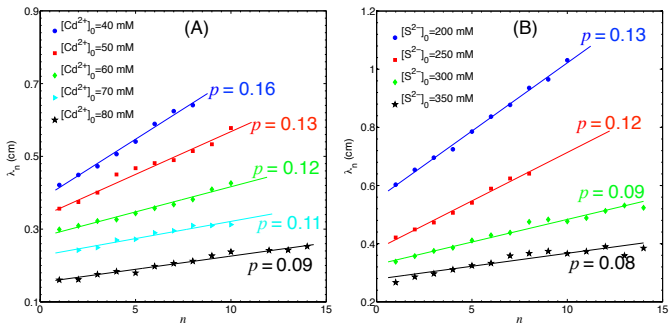

Fig. 6 Plots of the spacing between two consecutive spots λ_n versus the spot number (n). (A) represents *Set (I)* with fixed outer concentration $[S^{2-}]_0$ = 250 mM and different inner concentrations. (B) represents *Set (II)* with fixed inner concentration $[Cd^{2+}]_0$ = 60 mM and different outer concentrations. The spacing coefficient p for each case is also shown.

has gained a particular interest in recent years is the spinodal decomposition scenario adapted to precipitation pattern formation[31,32]. The formation of colloidal phase in this system prior to banding was recently investigated[33]. The gist of this theory is based on a phase separation scenario of colloidal particles that are first produced by the reaction. Under suitable conditions, these colloidal particles could subsequently phase separate into regions of low concentration (no precipitate) and high concentration (precipitate) leading to precipitation patterns. Such dynamics can be described by the nonlinear Cahn-Hilliard (CH) equation[34,35]. This formalism is shown to be suited to describe both the regular and the inverse banding in Liesegang-type precipitation patterns, and to reproduce many experimentally observed spacing laws such as the Matalon-Packter law[36].

The appearance of spots is explained on the basis of this aforementioned spinodal decomposition model. The processes that contribute to the dynamics are as follows. First, the irreversible mean-field reaction of the electrolytes A and B yields the reaction product C (A+B $\rightarrow$ C). Since the process takes place in a gel, no convection is present, and thereby it can be modeled as a simple reduced reaction-diffusion process:

$$\frac{\partial a}{\partial t} = \Delta a - kab \tag{1}$$

$$\frac{\partial b}{\partial t} = D\Delta b - kab \tag{2}$$

where a and b denote the dimensionless concentrations of the inner cadmium and outer hydroxide ions, $D = D_b/D_a$, D_a and D_b are their respective diffusion coefficients, Δ is the 2D Laplacian operator, and k is the precipitation reaction rate constant that is taken to be equal to 1 with appropriate choice of time and length scales. We also assume that the reaction of cadmium ions with the hydroxide ions (R_2) is bimolecular. We do not attempt in this model to incorporate the yellow back-front due to ion exchange in (R_3) as it can be simply described as a diffusion-controlled process, independent of the precipitation reaction. The reaction term (kab) provides the source for the precipitation of C, which takes the form of a diffusing front whose position, width, and shape are fully characterized[37]. This front leaves behind a constant density of C, denoted by c_0, which might subsequently undergo a phase separation[33,38]. The value of c_0 is determined by the initial concentration of A and B, a_0 and b_0, and by their diffusion coefficients[37]. The simplest form of the free energy$F[c]$ underlying the thermodynamics of this phase separation is assumed to have minima at some low c_l and high c_h concentrations. This function can be rewritten in terms of a shifted and rescaled concentration field $\varphi = (2c - c_h - c_l)/(c_h - c_l)$ and it is assumed to be of the following Ginzburg-Landau form over the spatial domain Ω:

$$F[\varphi] = \int_\Omega \left(-\frac{1}{2}\varepsilon\varphi^2 + \frac{1}{4}\gamma\varphi^4 + \frac{1}{2}\sigma(\nabla\varphi)^2 \right) d\Omega \tag{3}$$

where ε and γ are positive constants that define the boundary between the stable and metastable regions $\left(\varphi = \pm\sqrt{\varepsilon/\gamma}\right)$ and the spinodal line between the metastable and unstable regions $\left(\varphi = \pm\sqrt{\varepsilon/3\gamma}\right)$. If the front brings the system into the aforementioned unstable region, a precipitation pattern emerges as a result of spinodal decomposition scenario; otherwise, a uniform and stable continuous precipitation band is formed. The dynamics of the system is then described by the following CH equation with a source term:

$$\frac{\partial\varphi}{\partial t} = -\lambda\Delta(\varepsilon\varphi - \gamma\varphi^3 + \sigma\Delta\varphi) + ab \tag{4}$$

The parameters λ and σ are the rescaled kinetic coefficient and surface tension, respectively[31]. The ratio σ/λ defines a characteristic time scale of the growth of unstable modes in precipitation. In general, comparing this time scale with the time it takes for the front to pass through a certain region determines whether slow nucleation-and-growth (metastable region) or fast spinodal decomposition (unstable region) dominates the pattern formation[39], especially in the presence of internal fluctuations. Equations (1, 2, and 4) are solved numerically using a vertex-based finite volume method on unstructured meshes, whereby the spatial discretization is carried out using the control volume finite element method (CVFEM). The resulting nonlinear differential equations are successfully integrated using a fast and robust scheme based on operator splitting and a line search Jacobian-free Newton-Krylov method[40]. The structureless mesh, which is generated by the open source software *Triangle*[41], is suitable to reproduce the

RSC Advances Accepted Manuscript

This journal is © The Royal Society of Chemistry [year]

complex geometry of our circular reactor (Fig. 1). The initial conditions for a, b and φ are chosen such that $a_0 = a(t = 0) \gg b_0 = b(t = 0)$ and $\varphi_0 = \varphi(t = 0) = -1$, where a_0 is maintained at the inner circular boundary, and no-flux boundary conditions along the outer circular boundary are applied. In Fig. 7, for a given set of parameters, the numerical solution reveals the formation of Liesegang rings at the early stages of evolution (Fig. 7A) in the wake of a well-localized front that moves diffusively forward. The choice of $D_a > D_b$ is based on the fact that the gelatin matrix binds to the cadmium ions contrary to the diffusing outer hydroxide ions, which are more free to move, thus causing this difference in the magnitude of the diffusion coefficients[33,42]. The transition to spots takes place after the formation of a few rings (Fig. 7B) until the whole domain is filled with spots that coarsen with time in agreement with the experiment (Fig. 7C-D). The parameter space is then explored in order to locate a possible threshold beyond which such a transition is suppressed. It is noticeable that if the estimated φ_0 generated by the reaction front is in the unstable region but close to the spinodal line, only rings are obtained. On the other hand, the deeper the system penetrates into the unstable region away from the spinodal line, the faster the transition to spots occurs. In the case of Fig. (7), the threshold value is obtained for $\varepsilon = 1$ and $\gamma \approx 0.4$. This can be attributed to strong nonlinear coupling and interactions between unstable modes that can be expressed as patterns that are more complex than regular bands. The simulation also portrays the coarsening aspects of spots whose size as well as the wavelength of the hexagons/squares they form increases as the reaction front propagates forward. Moreover, the numerical results confirm the order of the appearance of the patterns '**C**', '**R**', '**S**', '**R**', and '**C**', respectively, as the inner concentration b_0 is increased at a fixed a_0. This in turn increases the concentration field φ_0[31] which corresponds to moving horizontally on the phase diagram at a given outer concentration. This order endorses the spinodal decomposition scenario in this system. However, we suspect that the reproduction of the '**R+s**' pattern numerically requires the incorporation of the inherent static disorder of the internal structure of the gel[43] in the parameters of the Cahn-Hilliard equation.

The authors gratefully acknowledge the funding provided by the American University of Beirut Research Board and by the Lebanese National Council for Scientific Research (LCNSR).

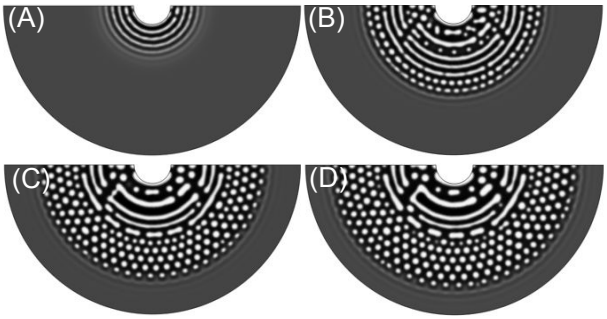

Fig. 7 Time evolution of the field φ exhibiting transition from Rings to Spots. (A) $t = 10$; (B) $t = 20$; (C) $t = 33$; (D) $t = 37$. Parameters are $k = 1, D_a = 5, D_b = 1, \sigma = 0.1, \lambda = 1, \varepsilon = 1, \gamma = 0.2$; initial conditions: $a_0 = 75$, $b_0 = 0.3$, $\varphi_0 = 0$ perturbed with 1% random noise. No-flux boundary conditions are applied at the external boundaries. The radius of the large circle is taken to be 8 times greater than that of the small circle. Number of elements is 11456.

References

1 E. O. Budrene and H. C. Berg, *Nature*, 1995, **376**, 49–53.
2 X. Serra-Picamal, V. Conte, R. Vincent, E. Anon, D. T. Tambe, E. Bazellieres, J. P. Butler, J. J. Fredberg and X. Trepat, *Nature Physics*, 2012, **8**, 628–634.
3 W. Hanke, d. L. V. M. Fernandes, M. Wiedemann and K. MeIssn-older, *Protoplasma*, 2006, **229**, 235–242.
4 W. Ngamsaad and K. Khompurngson, *Physical Review E*, 2012, **86**, 062901–1–062901–4.
5 V. I. Elokhin, A. V. Matveev and V. V. Gorodetskii, *Kinet. Catal.*, 2009, **50**, 40–47.
6 M. C. Cross and P. Hohenberg, *Reviews of Modern Physics*, 1993, **65**, 851–1112.
7 M. Orlik, *Journal of Solid State Electrochemistry*, 2009, **13**, 245–261.
8 R. E. Liesegang, *Naturwissenschaftliche Wochenschrift*, 1896, **11**, 353–362.
9 R. E. Liesegang, *Chemical Reactions in Gels*, Dusseldorf, 1898.
10 N. Kanniah, F. D. Gnanam, P. Ramasamy and G. S. Laddha, *Journal of Colloid and Interface Science*, 1981, **80**, 369–376.
11 S. K. Smoukov, I. Lagzi and B. A. Grzybowski, *The Journal of Physical Chemistry Letters*, 2011, **2**, 345–349.
12 L. Mandalian and R. Sultan, *Collect. Czech. Chem. Commun.*, 2002, **67**, 1729–1742.
13 A. Volford, F. Izsák, M. Ripszám and I. Lagzi, *Langmuir*, 2007, **23**, 961–964.
14 R. Suganthi, E. Girija, S. Narayana Kalkura, H. Varma and A. Rajaram, *Journal of Materials Science: Materials in Medicine*, 2009, **20**, 131–136.
15 I. T. Bensemann, M. Fialkowski and B. A. Grzybowski, *The Journal of Physical Chemistry B*, 2005, **109**, 2774–2778.
16 B. A. Grzybowski, K. J. M. Bishop, C. J. Campbell, M. Fialkowski and S. K. Smoukov, *Soft Matter*, 2005, **1**, 114–128.
17 I. Lagzi, *Langmuir*, 2012, **28**, 3350–3354.
18 H.-J. Krug and H. Brandtstadter, *The Journal of Physical Chemistry A*, 1999, **103**, 7811–7820.
19 E. Kuster, *Kolloid Zeitschrift*, 1914, **14**, 307–319.
20 R. Matalon and A. Packter, *Journal of Colloid Science*, 1955, **10**, 46–62.
21 L. Badr and R. Sultan, *The Journal of Physical Chemistry A*, 2009, **113**, 6581–6586.
22 Z. Shreif, L. Mandalian, A. Abi-Haydar and R. Sultan, *Physical Chemistry Chemical Physics*, 2004, **6**, 3461–3466.
23 H. Morse and G. Pierce, *Physical Review*, 1903, **17**, 129.
24 M. Droz, *Journal of Statistical Physics*, 2000, **101**, 509–519.
25 W. Ostwald, *Lehrbuch der Allgemeinen Chemie*, Engelmann: Leipzig, Germany, 1897.
26 S. Prager, *The Journal of Chemical Physics*, 1956, **25**, 279–283.
27 G. Venzl, *The Journal of Chemical Physics*, 1986, **85**, 1996–2005.

RSC Advances Accepted Manuscript

28 G. Venzl, *The Journal of Chemical Physics*, 1986, **85**, 2006–2011.

29 I. M. Lifshitz and V. V. Slyozov, *Journal of Physics and Chemistry of Solids*, 1961, **19**, 35–50.

30 D. S. Chernavskii, A. A. Polezhaev and S. C. Müller, *Physica D: Nonlinear Phenomena*, 1991, **54**, 160–170.

31 T. Antal, M. Droz, J. Magnin and Z. Rácz, *Physical Review Letters*, 1999, **83**, 2880–2883.

32 Z. Racz, *Physica A: Statistical Mechanics and its Applications*, 1999, **274**, 50–59.

33 M. Al-Ghoul, T. Ghaddar and T. Moukalled, *The Journal of Physical Chemistry B*, 2009, **113**, 11594–603.

34 J. W. Cahn and J. E. Hilliard, *The Journal of Chemical Physics*, 1958, **28**, 258–267.

35 J. W. Cahn, *Acta Metallurgica*, 1961, **9**, 795–801.

36 T. Antal, M. Droz, J. Magnin, Z. Rácz and M. Zrinyi, *The Journal of Chemical Physics*, 1998, **109**, 9479–9486.

37 L. Gálfi and Z. Rácz, *Physical review. A*, 1988, **38**, 3151–3154.

38 E. Foard and A. Wagner, *Physical Review E*, 2012, **85**, 011501.

39 S. Thomas, I. Lagzi, F. Molnár and Z. Racz, *Physical Review Letters*, 2013, **110**, 078303(1)–078303(5).

40 A. Abi Mansour and M. Al-Ghoul, *Physical Review E*, 2014, **89**, 033303.

41 J. R. Shewchuk, *Computational Geometry*, 2002, **22**, 21–74.

42 M. Al-Ghoul and T. Ghaddar, *Journal of Nano Research*, 2010, **11**, 19.

43 J. Rahbani, A. R. Behzad, N. M. Khashab and M. Al-Ghoul, *Electrophoresis*, 2013, **34**, 405–408.

RSC Advances Accepted Manuscript

This journal is © The Royal Society of Chemistry [year]

TOC Graphic

RSC Advances Accepted Manuscript